Journal of
Composites Science

MDPI

Article

Investigation on Magnetization, Magnetocalory, Magnetoresistance, and Electric Properties of Ni-Mn Based Heusler Alloy

Sandeep Nambiar S. [1], Murthy B. R. N. [1,*], Karthik B. M. [1,*], Sathyashankara Sharma [1] and A. A. Prasanna [2]

[1] Department of Mechanical and Industrial Engineering, Manipal Institute of Technology, Manipal Academy of Higher Education, Manipal 576104, Karnataka, India
[2] Department of Physics, Malnad College of Engineering, Hassan 573202, Karnataka, India
* Correspondence: murhty.brn@manipal.edu (M.B.R.N.); karthik.bm@manipal.edu (K.B.M.); Tel.: +91-9620867499 (M.B.R.N.); +91-9632258010 (K.B.M.)

Abstract: The magnetic and electrical characteristics of Ni-Mn quinary Heusler alloys are studied in the current work. The results concern the materials' magnetic and electrical behavior. The physical property measurement system (PPMS) and superconducting quantum interference device (SQUID) were used at various magnetization levels to determine the results. The addition of Fe helps to form the alloy into a smart memory alloy with magnetocrystalline anisotropy, twin border mobility, and varied magnetic and martensite transition temperature characteristics. Character changes in the superparamagnetic (SPM) and paramagnetic (PM) alloys occur between 26 and 34 °C. The curves are supported by the alloy's martensitic transition temperature change. A large refrigeration capacity is identified in the alloy. These properties are an indication of the alloys' application prospects. Entropy change helps to detect the inverse magnetocaloric effect in the alloy, whereas adiabatic temperature change helps identify the origin and validity of reverse magnetic properties. The transition temperature changes occur when austenite's sigma is larger than that of martensite, and as the magnetic field increases, the temperature declines. Isothermal magnetization curves, a large (MR)/B value at low and high magnetic fields, and temperatures near the transformation point suggest that small-crystal Heusler alloys have tremendous promise for low and high magnetic field magnetoresistance applications.

Keywords: magnetization; magnetocalory; magnetoresistance; electric property; Heusler alloy

Citation: Nambiar S., S.; B. R. N., M.; B. M., K.; Sharma, S.; Prasanna, A.A. Investigation on Magnetization, Magnetocalory, Magnetoresistance, and Electric Properties of Ni-Mn Based Heusler Alloy. *J. Compos. Sci.* **2023**, *7*, 5. https://doi.org/10.3390/jcs7010005

Academic Editor: Francesco Tornabene

Received: 22 October 2022
Revised: 28 November 2022
Accepted: 2 December 2022
Published: 27 December 2022

1. Introduction

The growing demand for alternate cooling technology has encouraged researchers to look for alternatives, and among these are smart memory alloys (SMA) [1,2]. These alloys tend to show interesting properties around their transformation temperatures that can be suitable for refrigeration-related applications. The magnetic, magnetocaloric, inverse magnetocalory, and isothermal magnetization properties are some of the properties that are of great interest among researchers [3–6]. Among the alloys, Ni-Mn-based alloys are most commonly used since they show tremendous application prospects [7–10]. The complete Ni-Mn-based Heusler alloys are the most investigated Heusler alloy systems. In terms of magnetocalory, an essential series of ferromagnetic shape memory (FSM) alloys is the ferromagnetic Ni-Mn-based Heusler alloys. These alloys undergo a martensite transition from a high-temperature parent austenite phase to a low-temperature martensite phase across a wide composition range. Magnetic and structural transitions coexist in this transition, as does a small thermal hysteresis [11–13]. The SMAs exhibit the expected magnetocrystalline anisotropy, strong twin border mobility, and tunable magnetic and martensite transition temperatures. The transformation temperature is greatly controlled by the composition and electron concentration, and heating procedure also has a considerable impact on the

stability of the martensitic structure and transformation temperature in ferromagnetic shape memory alloys. Researchers investigated the impact of a longer annealing period on the magnetic order and martensitic transition temperatures of Ni-Mn alloy. They discovered that annealing had a significant effect on both the magnetic order and martensitic transition temperatures of Ni-Mn-based alloy. Numerous researchers have determined that the temperature range of 3 h for 700–800 °C is the optimal range for annealing Ni-Mn-based Heusler alloys. As martensite transition is observed in the cubic $L2_1$ type crystal structure to orthorhombic four-layered martensite (4O) Heusler alloys, there has been a great deal of interest in investigating the structural transitions, magnetoelastic properties, and magnetic conductivity properties in the materials in the past few years. The crystal structures as well as the characteristic temperatures of the mutual reversible transition are extremely sensitive to the e/a value, which varies depending on the microstructure of the crystal [14–18]. Because of its increased characteristics, application aspect, simplicity of availability, and cost efficiency, Ni-Mn-Sn-based Heusler alloys have long been popular within the Heusler alloy family [19–22]. The heat treatment characteristics of quinary Heusler alloys based on Ni-Fe-Mn-Sn-In are being researched because they exhibit strong shape memory and thermal properties [23–25]. The composition of the alloy determines its martensitic transformation characteristic [8–13]. Additionally, the annealing time and temperature are of greater importance with regard to the martensitic transformation of the alloy [26–28].

In this manuscript, we investigate the extension of our previous results of mechanical characteristics to the magnetic and electric property testing of the alloy. We have seen that the addition of Fe as the constituent element significantly enhances the alloy's mechanical properties. This paper gives an in-depth analysis of these properties, and the dependence of the compositional change on the alloy's behavior and a co-relation amongst it is established.

2. Materials and Methods

These alloys' magnetocaloric performance is optimized primarily via compositional analyses, mainly as the transition temperatures are largely composition dependent. For instance, the martensitic transition in the Ni-Mn alloy series rises as the electron per atom concentration (e/a) increases. The electron concentrations in the outer shells can be calculated according to Equation (1).

$$e/a = (10 \times (\text{Ni at.\%}) + 7 \times (\text{Mn at.\%}) + 4 \times (\text{Sn at.\%}) + 8 \times (\text{Fe at.\%}) + 3 \times (\text{In at.\%}))/100 \quad (1)$$

Samples of alloys weighing 5 g each were created in an argon environment utilizing just a vacuum arc melting furnace in a water-cooled copper (Cu) crucible. After determining the concentrations of Ni, Mn, Fe, Sn, and In (99%), the specimen was loaded into the hearth chamber and the chamber was prepared by removing any traces of oxygen. To minimize mass loss during the melting process due to the evaporation of the component metals with low melting points, the pure metals were layered in a crucible in decreasing order of their melting temperatures. This helps in the melting of low melting temperature metals by absorbing the heat from the melt of a high melting temperature metal laying on top of them. The specimens thus formed were later subjected to annealing at 800–850 °C for 48 h, after which the furnace was turned off and the specimen allowed to drop gently to room temperature. To bring the temperature down to room temperature, the cooling procedure takes 20–24 h.

To determine the magnetic property of the alloy, the physical property measurement system (PPMS) 14 T from Quantum Design was used. A vertical scanning magnetometer (VSM), electrical transport option (ETO), resistivity, heat capacity, and thermal conductivity tests were conducted. The superconducting quantum interference device (SQUID) magnetometer and magnetic properties measurement system (MPMS) equipment were used in the study. The operating temperature range was within the range of −271 to 126 °C with an operating magnetic field range of ± 14 kOe. The phase transitions, magnetic resonance, and electronic transport in alloys were determined as a function of two physical factors, B

and temperature. A tiny rectangular bar (10 × 2 × 1 mm) of a flat sample was employed for these measurements. The sample was handled carefully to ensure adequate contact between the four probes and the surface. The magneto resistance (MR) properties of the alloys was investigated in detail using a PPMS that enabled the measurement of the value in magnetic fields up to 10 T across a broad temperature range of −271 to 126 °C. A direct current of 100 mA was supplied parallel to the length of a bar in both alloy series.

To investigate the magnetocaloric effect (MCE), the heat capacity of the alloys was measured using the PPMS throughout a temperature range at zero field and in fields up to 14 T. After chilling a sample in a zero magnetic field, the measurements were made. Despite the MCE, the heat capacity measurements give important information on a sample's lattice, electronic, and magnetic characteristics. Heat capacity measurements directly probe a material's electronic and magnetic energy levels, allowing for the comparison of the theoretical and experimental data necessary for determining the mechanism of magnetocaloric characteristics. Practically speaking, every material utilized in the construction of thermal devices such as freezers or cryostats must be properly described in terms of heat capacity, enthalpy change, and a variety of other physical properties.

The PPMS regulates the amount of heat delivered to and withdrawn from a sample during a measurement, while measuring the resultant temperature change at a constant pressure. A consistent quantity of heat is applied to the sample for a specified period, followed by a cooling cycle of the same length. The measurement entails determining the sample's total heat capacity. Two measurements, one with and one without a sample on the sample platform, are required to obtain a result with a 0.01 mJ/gK error bar. To obtain an accurate reading, we put a small quantity of grease on the sample platform, just enough to retain the sample, and then tested the heat capacity of both the grease and the platform. Following that, we mounted a sample of 3 mg mass on the platform by pushing it against the grease and then measured the heat capacity extremely accurately within an error bar of 0.01 mJ/kg.

3. Results

The alloy's mechanical and martensitic transformation characteristics have been previously studied extensively in [28–31]. The following test results are presented to establish their relationship with the previous study.

3.1. Isothermal Magnetization

To determine the superparamagnetic (SPM) and paramagnetic (PM) nature changes in the alloys with respect to σ-B curves, the curves are measured at temperature range between 26 and 34 °C as the temperature range covers the martensite to austenite transition with B(T) from 0–5 T, as shown in Figure 1. A selective temperature interval range is taken to determine the martensitic transformation occurring in the material. All of the formed curves show a ferromagnetic shape memory over the temperature range. The data were derived by heating the ZFC alloys samples from a set temperature point to a point below the transformation temperature. We see that the alloy with x = 4 shows a σ of around 30 emu/g from a temperature of 20–30 °C at 5 T. From the literature, a refrigerant capacity (RC) Formula (2) is identified where RC helps in measuring the heat transferred between the cold and hot sink in one refrigeration cycle of the specimen.

$$\mathrm{RC} = \int_{T1}^{T2} \Delta S_m(T) B \, dT \tag{2}$$

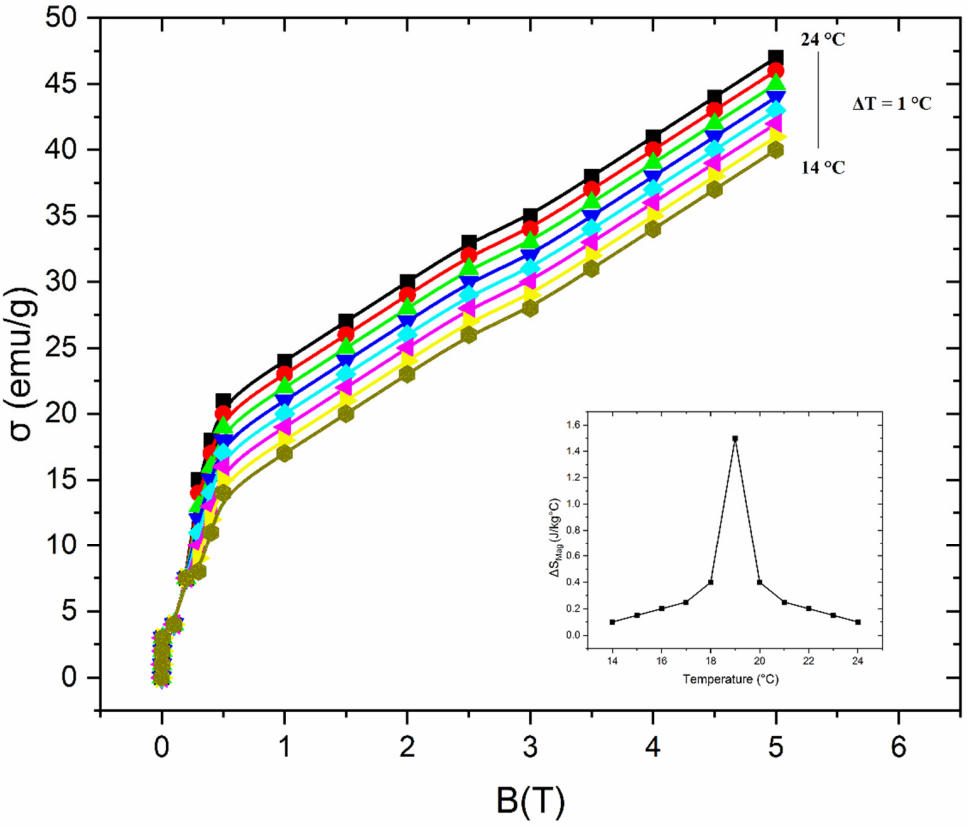

(**a**)

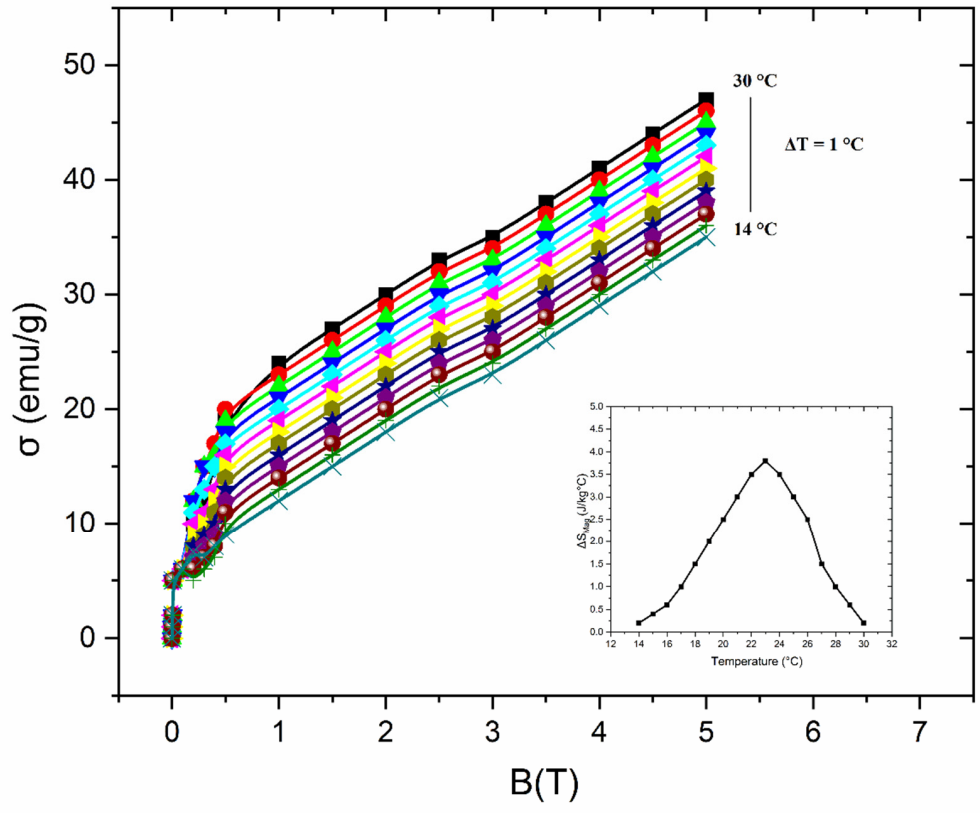

(**b**)

Figure 1. *Cont.*

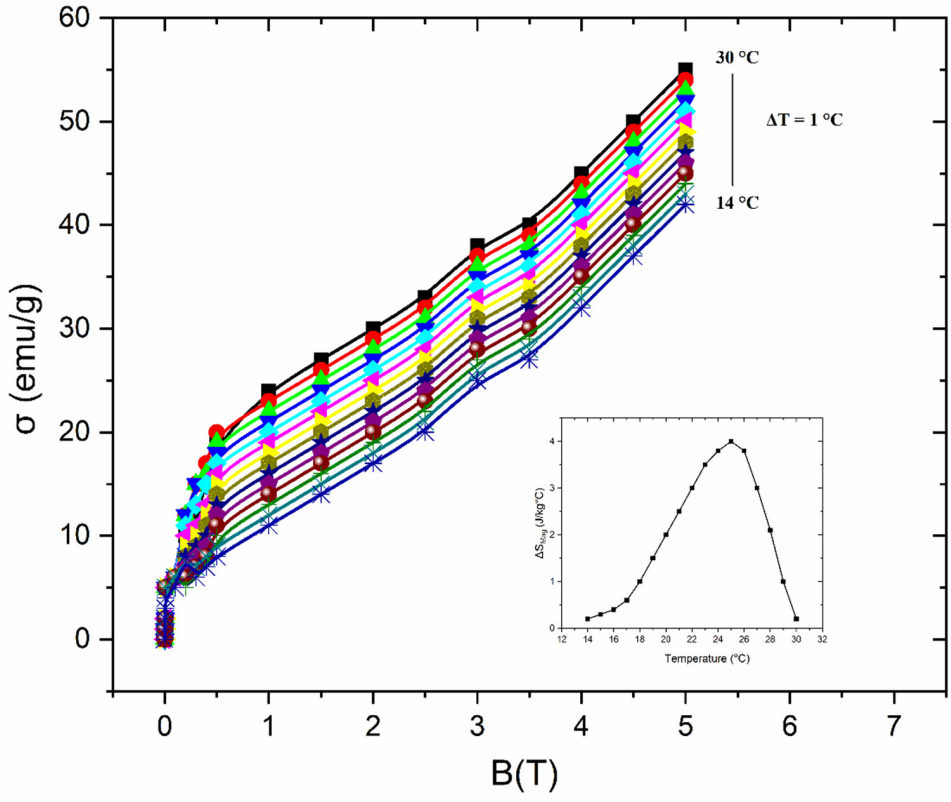

(**c**)

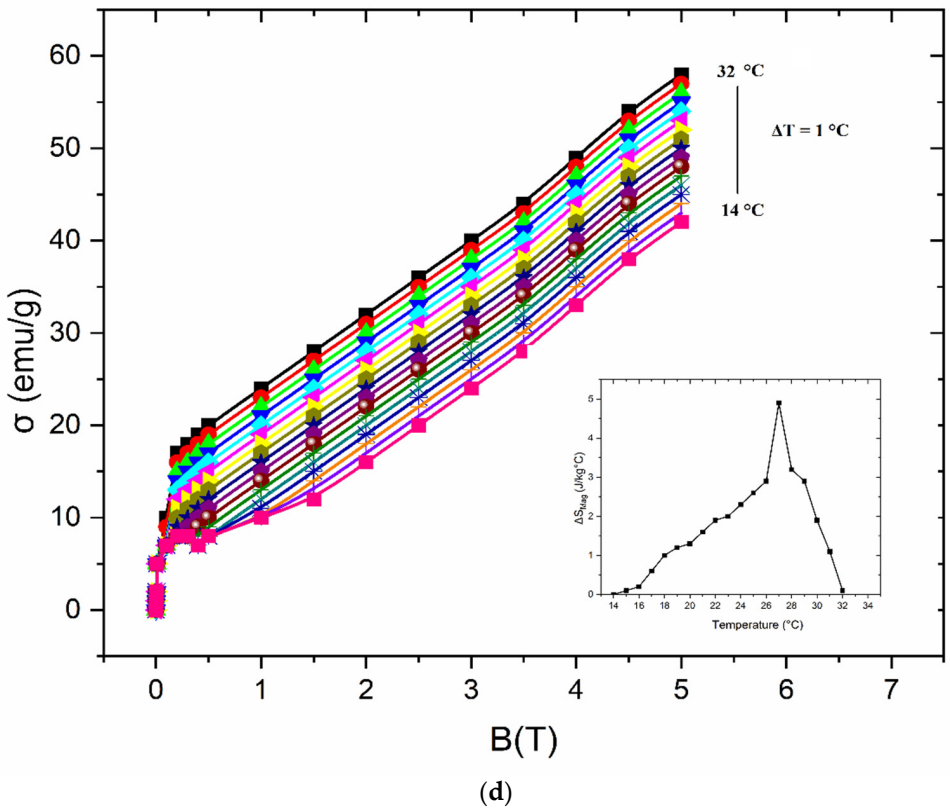

(**d**)

Figure 1. Isothermal magnetization plots for alloy sets where for $Ni_{50-x}Fe_xMn_{30}Sn_{20-y}In_y$, $1 \leq x \leq 4$; $2 \leq y \leq 8$ alloy and (**a**) x = 1, y = 2; (**b**) x = 2, y = 4; (**c**) x = 3, y = 6; and (**d**) x = 4, y = 8.

For the change in flux ΔB = 5 T in (2), we obtain RC = 130 J/kg at TA = 33 °C point in the alloy with x = 4. Such a large RC value and the change in entropy (ΔS_m) arise in

correlation to the residual strain, which is relieved mainly when an alloy comprises single-phase mall crystallites, as per Prasanna et al. [32]. Such crystallites convert from austenite to martensite nearly completely. A substantial residual strain (3.5%) in a mixed-phase alloy (x = 3) reduces ΔS_m, a main cause of its loss, to 3.5 J/kg-K. When austenite and martensite coincide, the inverse MCE effect in the martensite transition is reduced. Only a single-phase martensite alloy may produce a big ΔS_m. As predicted, the isothermal curves show a larger value of σ. Thus, we observe that the larger RC value found in alloys with x = 4 substitution is mainly useful in refrigeration applications. It can also be co-related to the larger ΔS_m value seen associated with it that further strengthens the observation.

3.2. Temperature Dependence of Heat Capacity

The temperature variation of the heat capacity (Cp) is used to determine both entropy change (S_m) and adiabatic temperature change (T_{ad}) in the alloys. The value of S_m helps in identifying the value change of the inverse MC effect in the alloy, and the adiabatic temperature change along with σ helps in identifying the origin and the validity in the magnetic properties, as shown in Figure 2i. here, the Cp vs. T variation of the various sets of alloys is shown: a) depicts the alloy at x = 4 and y = 8, over a temperature range of −200 to 150 °C while the alloy is in a pure martensitic state during both the cooling and heating cycle at 0, 5, and 10 T field. From the plot, it is seen that the transformation of M–A occurs at As of around 15 °C and moves towards 24 °C. The sigmoid shape of the plot shows that the Cp value reaches a peak of 600 J/kg °C with a steady rise from 0.5 J/kg °C. At the point of transition, there is a decrease in the slope and it approaches a value of around 500 J/kg °C. A peak forming in the Cp during the martensite to austenite transition becomes suppressed during cooling in a reverse transition.

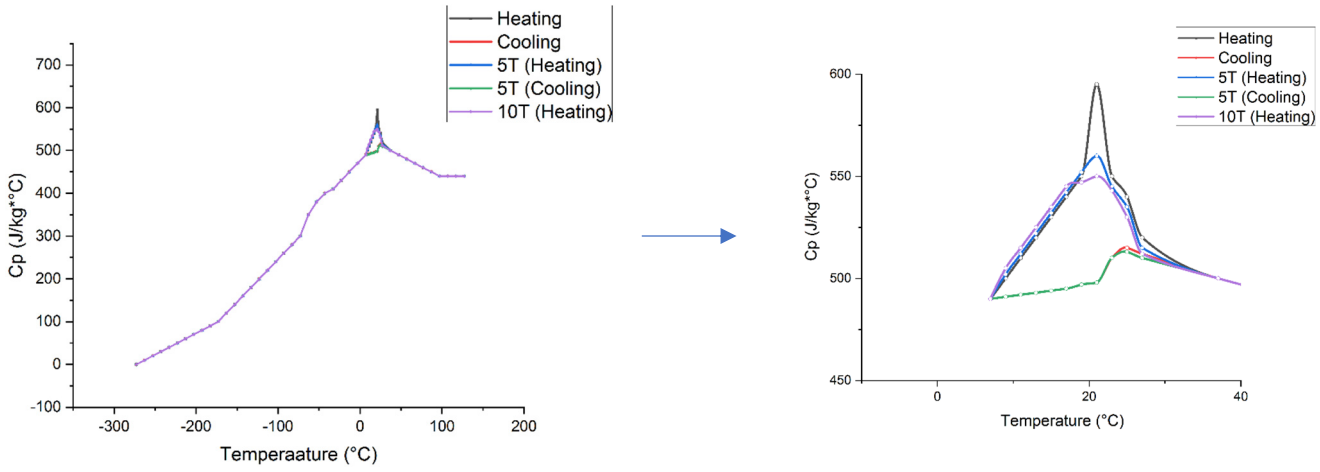

Figure 2. (**a**) Cp vs. temperature for alloy with Fe_4 concentration; (**a(i)**) represents the magnified image.

The plot shows a peak in the zero-field heating for the Cp at around 590 J/kg °C. While the specimen is reheated at a higher field rate, we see a shift in the peak to around 575 J/kg °C. When the specimen is applied with a suppressive B to attain a ferromagnetic order, we see a shift in the curve and the curve attains stability. The zoomed-in region of the curve clearly shows dips in the change in the transformation temperature with the variation in the field applied from 0 to 10 T, as seen in Figure 2a(i).

The variation in the transformation temperature with the variation in Cp varies with the change in B. Such a predominant shift is observed when the sigma value of the austenite phase is higher than the martensite phase. The martensite phase transition is formed by the phonon variation at the transformation temperature point. The increase in the sigma value with B favors the transformation phase of the cubic structure, finally leading to a gradual

reduction of the phonon instability due to linking between the magnetic and vibrational degree of freedom [33]. This is depicted by the reduction in the transition temperature along with the increase in B, as shown in Figure 3.

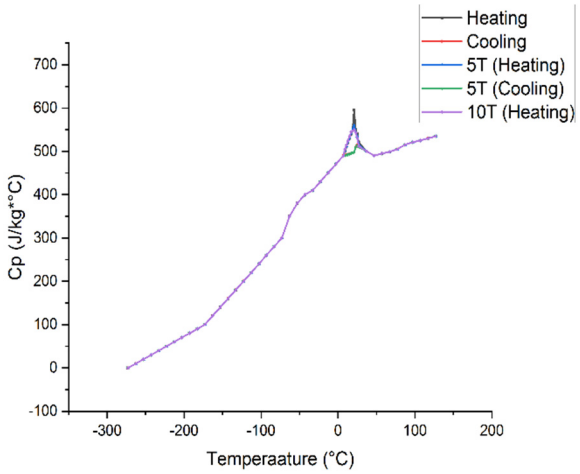

(**b**)

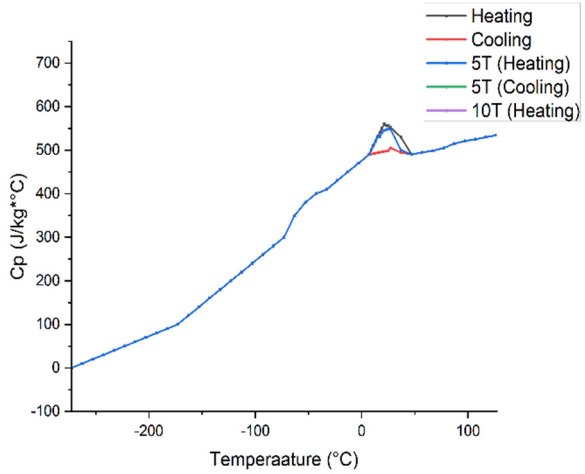

(**c**)

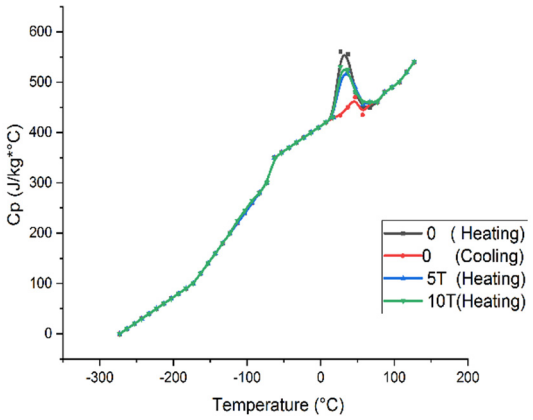

(**d**)

Figure 3. Cp vs. temperature for (**b**) alloy with Fe_3, (**c**) alloy with Fe_2, and (**d**) alloy with Fe_1 concentration.

3.3. Field Dependence Inverse Magnetocalory

The ΔS_m and T_{ad} graphs, as seen in Figure 4, are plotted over temperature, obtained from Equations (2) and (3), for four alloy compositions.

$$\Delta S_m = S(T)_{BF} - S(T)_{BO} \quad (3)$$

$$\Delta T_{ad} = T(S)_{BF} - T(S)_{BO} \quad (4)$$

where BF and BO are the initial and final values of the applied field B, and $S(T)_{BF}$ and $S(T)_{BO}$ are calculated using the indirect method measure equation as in Prasanna et al. [33]. Expectedly, ΔS_m is the highest in single-phase crystallite alloys. The values peak at the TM (or TA) transition point, showing rapid atomic redistribution in tiny crystallites. Concurring two austenite–martensite alloy phases in a lower Fe-containing sample (x = 1 and x = 2) reduces Sm. Small values persist because the transition generates a non-equilibrium state, hindering spin dynamics. Even with a higher field B = 10 T, the S_m value is less than in x = 1 and x = 2 substituted alloys. The cooling and heating cycle effect from ΔS_m and ΔT_{ad} was also studied. As the transition mechanism lacks reversible spin ordering, only

67–92% of a cooling cycle's value emerges in a heating cycle (identical conditions). The two ΔS_m readings match within 0.2 J/kg-K. The large thermodynamic parameters ΔS_m suggest that an alloy with x = 4 substitution with its crystallites might be used as a magnetic refrigerant. In Figure 4, the two sets of acquired findings are shown with the x and y values representing their stoichiometry. The changes in the values are relatively close to one another, showing the validity of the model's thermodynamic relations in these alloys condensed into microscopic crystallites [32–34].

3.4. Electric Transport and Magnetoresistance

To determine the electric transport properties of the alloy, the alloys were formed into small sections and the resistivity (ρ) value was measured as a function of temperature across a temperature range from −271 to 120 °C at various field ranges from B from 0 to 10 T, as shown in Figure 5. The obtained results are plotted. To form the plot, the samples were measured in the zero-field cooled from the temperature range from −271 °C before the ρ values were measured during the applied magnetic field. On cooling the samples from the temperature of 120 °C for x = 4 and y = 8, the value for ρ remains in the region of around the resistivity (μΩ-cm) of 400, while the martensite start (Ms) temperature is around 37 °C. Once the M–A transition occurs, the change in ρ is seen to have a steep rise. While the sample is reheated to 271 °C, the samples continue to retain the value of α. The austenite start (As) temperature initiates at the M–A transition and terminates at the austenite finish (Af) temperature. When the heating is continued, the austinite phase retains the initial ρ above the Af temperature. Under an increased field of 5 and 10 T, the ρ value reduces to a lower section. Even during this phase, the temperature range of the section is similar to that of the zero-field ρ–T plot.

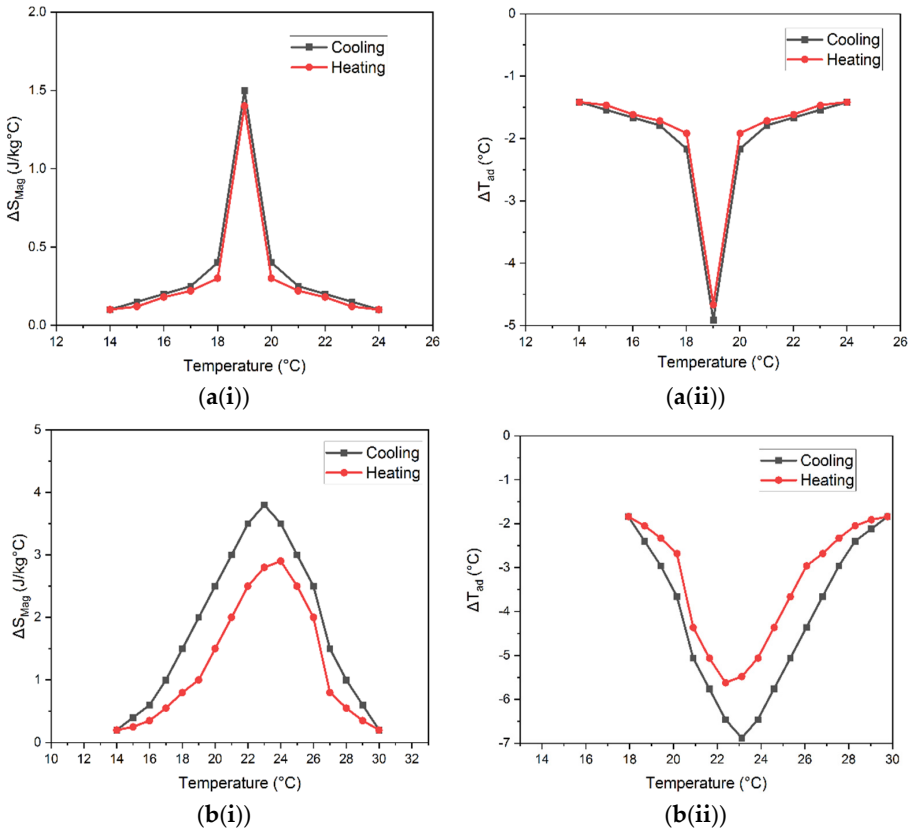

Figure 4. *Cont.*

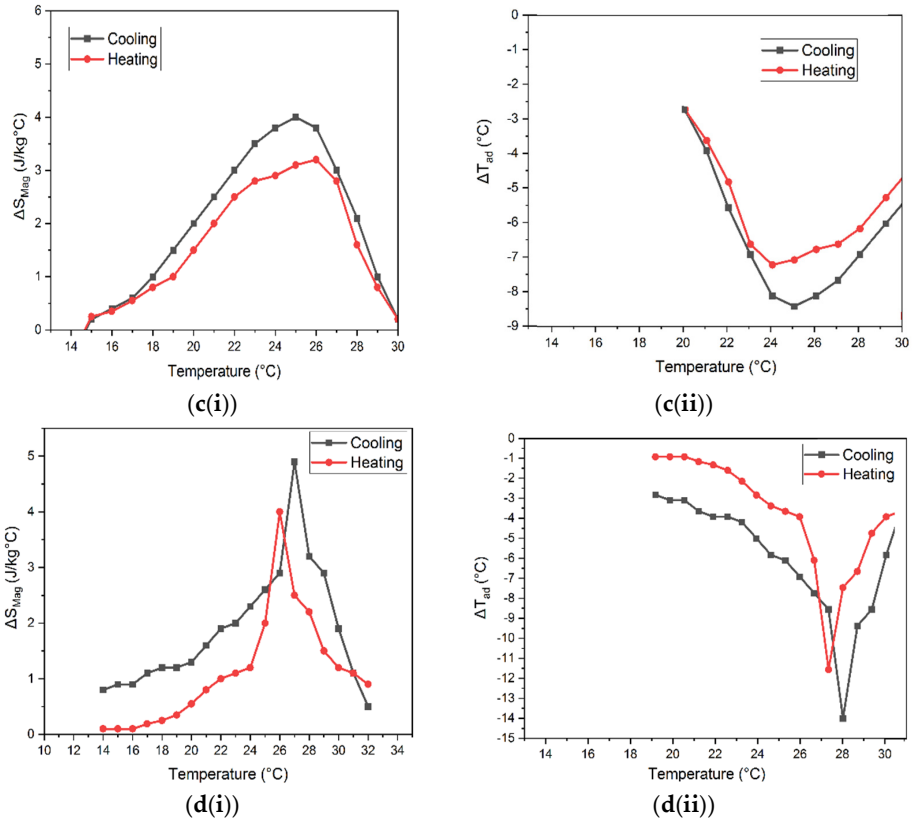

Figure 4. Field dependence inverse magnetocalory for alloys where for $Ni_{50-x}Fe_xMn_{30}Sn_{20-y}In_y$, $1 \leq x \leq 4$; $2 \leq y \leq 8$ alloy and (**a**) x = 1, y = 2; (**b**) x = 2, y = 4; (**c**) x = 3, y = 6; and (**d**) x = 4, y = 8, and i and ii represent ΔS_m and ΔT_{ad}, respectively.

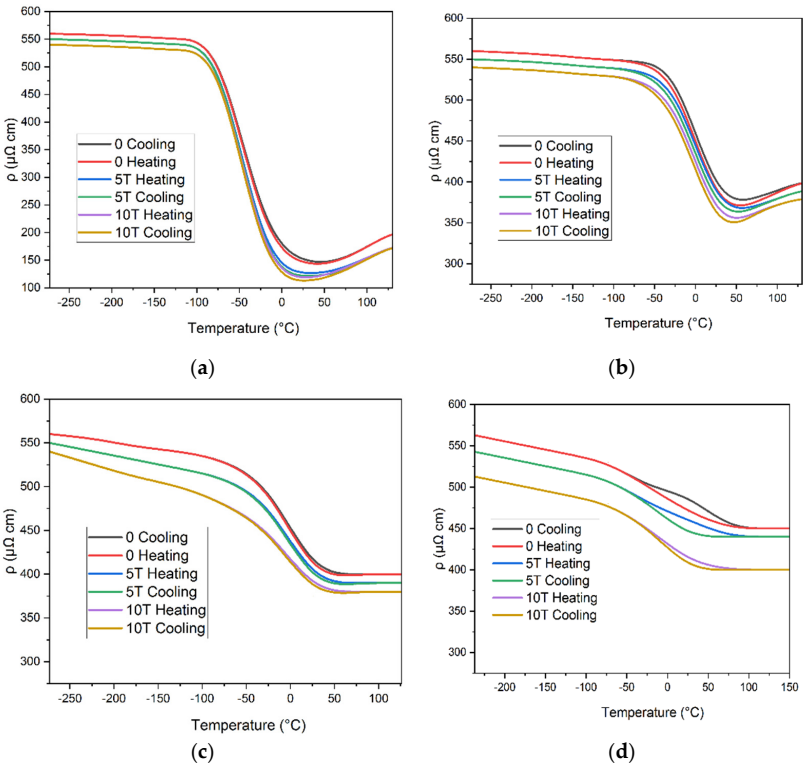

Figure 5. Electric transport property for $Ni_{50-x}Fe_xMn_{30}Sn_{20-y}In_y$ where $1 \leq x \leq 4$; $2 \leq y \leq 8$ alloy and (**a**) x = 1, y = 2; (**b**) x = 2, y = 4; (**c**) x = 3, y = 6; and (**d**) x = 4, y = 8.

When considering the case of Figure 5, we see that the change in stichometry concentration in the ρ value increases the martensite phase in the alloy by 12%. The various other transition parameters for the ρ vs. T plot are shown. The plot enables the identification of the curve behavior during the transformation in the martensite phase, the transition zone, and the austenite phase. The dependence of ρ on the transition and the temperature changes that occur accordingly are also seen.

3.5. Negative Magnetoresistance

The temperature fluctuation of the negative MR in the alloys is shown using the conventional relationship {(ρB − ρo)/ ρo} × 100, where ρB and ρo are the ρ in an applied field B and zero field, respectively. The MR values at the transition region are at the lowest (−273 °C) and highest (126 °C) temperatures used in the current measurements. At x = 4, y = 8, and B = 5 T, an MR value acquired in this manner has a magnitude of (−)20% in the M–A transition (TM °C), but a comparatively decreased magnitude of (−)17% in the reversed transition throughout the heating cycle. While we see that in case of x = 1, y = 2, the magnitude of MR% is at 14% and 11% for the cooling and heating cycle, respectively, as shown in Figure 6.

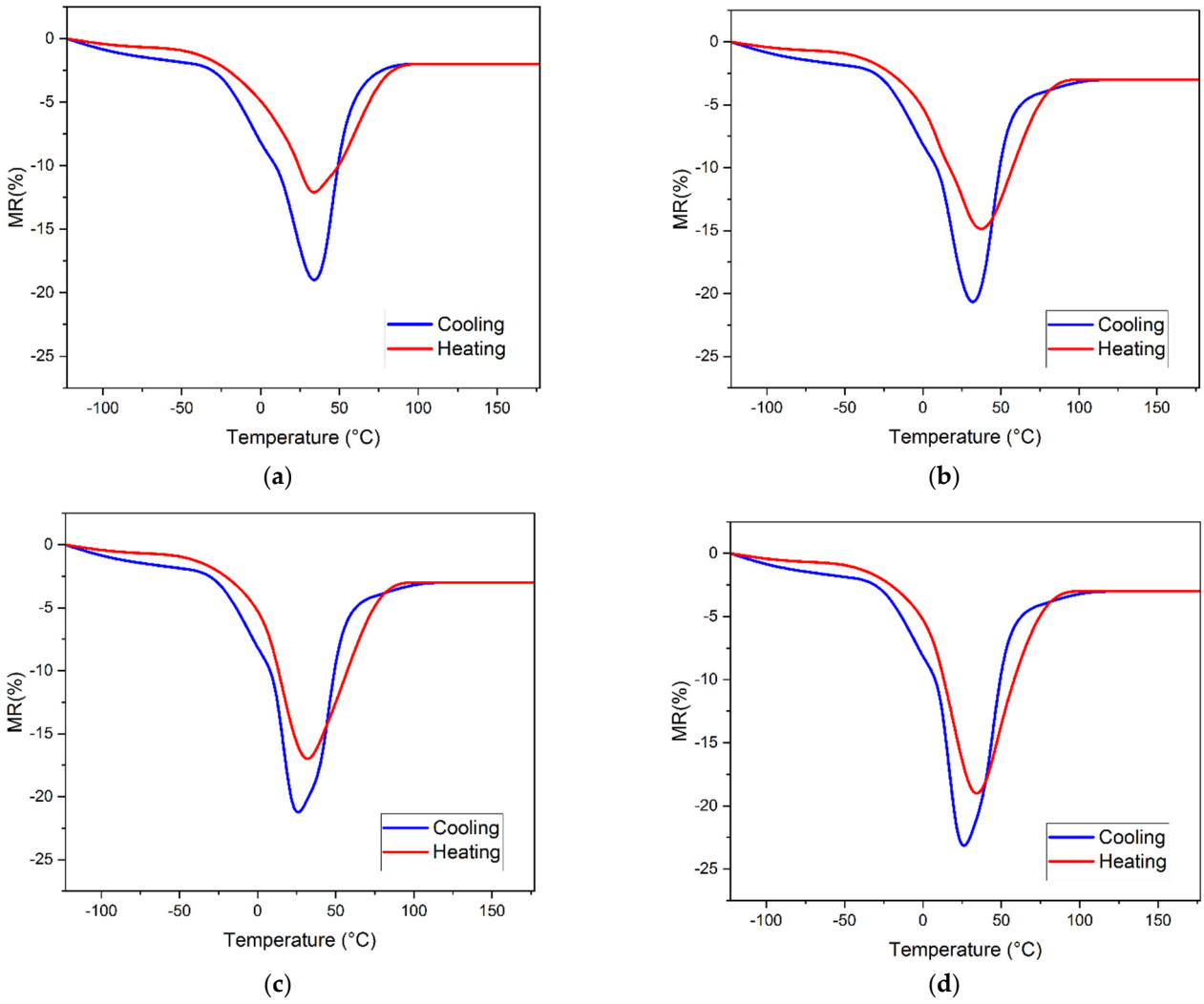

Figure 6. Negative magnetoresistance at the 5 T applied field for $Ni_{50-x}Fe_xMn_{30}Sn_{20-y}In_y$, where $1 \leq x \leq 4$; $2 \leq y \leq 8$ alloy and (**a**) x =1, (**b**) x = 2, (**c**) x = 3, and (**d**) x = 4.

In such a case, the spin disorder scattering from the domains is rapidly reduced and the likelihood of scattering by the formed strips is virtually zero. Eventually, the instantaneous

negative value decreases, resulting in an MR value that is essentially enormous. The alloy specimen must undergo a transformation from a spin-disordered PM state to a reordered FM state, as well as from the well-grown martensite phase to the austenite phase, during the M–A transition. Clearly, the suppression rates of spin-disorder scattering and twin-boundary scattering decrease, resulting in a significantly reduced MR value. This is due to the high irreversibility of spin reordering during the M–A transition. The irreversibility of MR is critical for magnetic memory systems, which store information by generating a low resistive state with an appropriate magnetic field.

3.6. Isothermal Magnetoresistance

To obtain a better understanding of the magnetic resonance behavior of the alloys at a particular temperature and to confirm the findings obtained from the ρ-T curves, the function of the magnetic field B swept up to 10 T at temperatures ranging from −173 to 70 °C was analyzed. The measurement was conducted after cooling the sample to −173 °C from room temperature using zero-field cooling. Plots of the MR values obtained from the ρ-B data versus B can be seen in Figure 7.

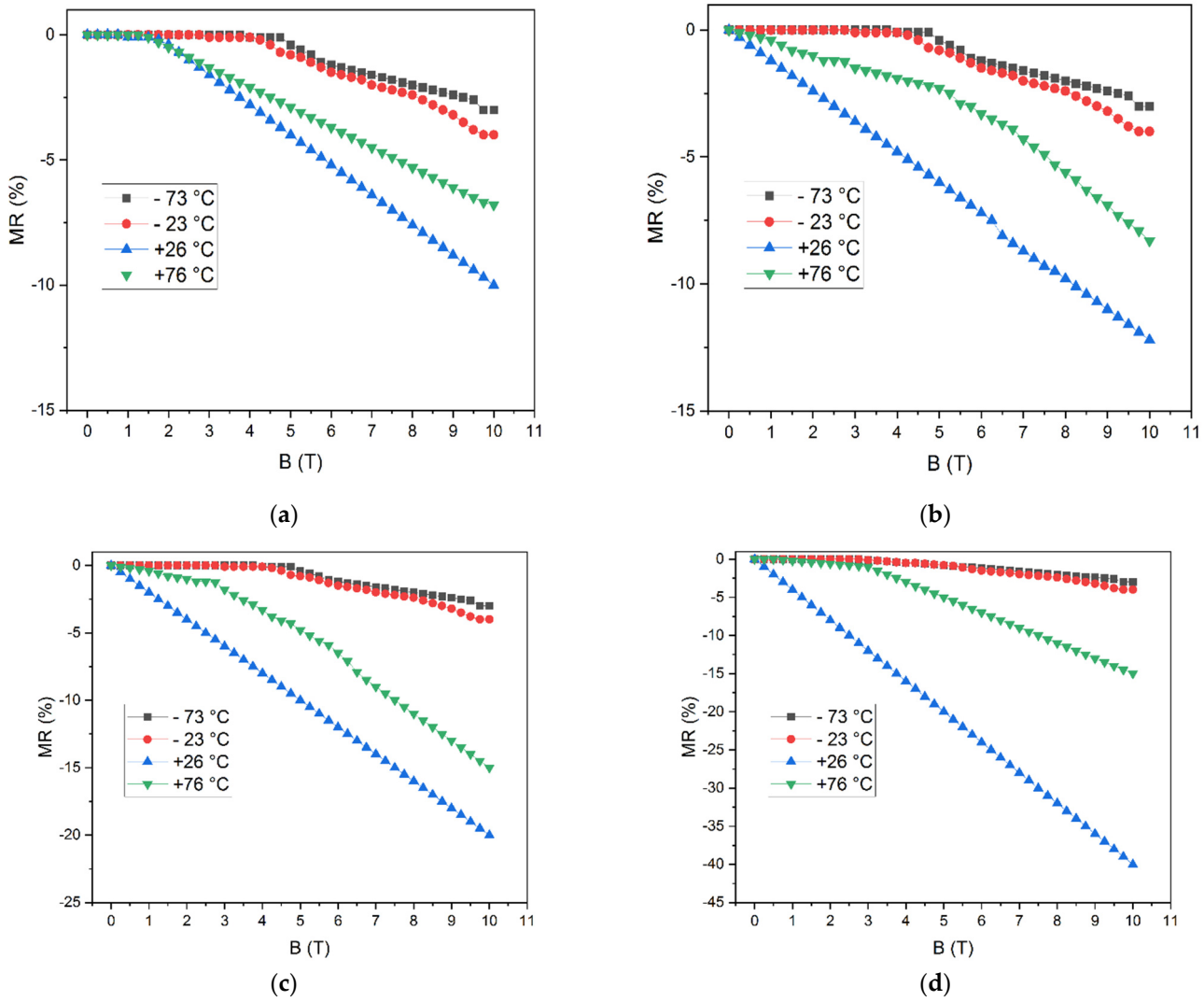

Figure 7. Isothermal magnetoresistance for $Ni_{50-x}Fe_xMn_{30}Sn_{20-y}In_y$, where $1 \leq x \leq 4$; $2 \leq y \leq 8$ alloy and (**a**) x =1, (**b**) x = 2, (**c**) x = 3, and (**d**) x = 4.

All samples indicate a linear relationship between the negative MR and B with a temperature-dependent slope Δ(MR)/B. At low temperatures, when the sample is in the

martensite phase, the value of (MR)/B is minimal due to its paramagnetic (SPM) state. For instance, in the alloy with x = 4 and y = 8 at a temperature of T = −173 °C, when the sample is in the PM state, the (MR)/B is 1.12%/T. This value is almost the same in the PM regions, i.e., at T = −73 and −23 °C. At the SPM to PM transition temperature of −23 °C, the value rises significantly by 26%. The (MR)/B is still more than 2.4%/T at T = 46.85 °C and 2.64%/T at T = 66.85 °C in the magnetically and structurally unstable martensite transition area. A significant shift in the magnetic and electronic structures associated with the martensite transition might present itself in the form of a big (MR)/B value or a large negative MR.

The MR values shown versus the temperature show similar tendencies for the other alloy compositions with tiny crystallites. When the alloy (x = 3 and y = 6) is heated to the austenite phase of 26 °C, the (MR)/B ratio is 16% less than that seen around the martensite transition point of 19 °C. This is clearly due to the spin ordering present in the austenite phase. The presence of a rather substantial (MR)/B value at both low and high magnetic fields and temperatures near to the TA point indicates that the current Heusler alloys composed of tiny crystallites have considerable promise for both low and high magnetic field MR applications.

4. Discussion

The results clearly indicate that with the change in the stochiometric composition of the alloy by the inclusion of Fe, the alloys tend to behave as an SMA. The alloys tend to exhibit the expected magnetocrystalline anisotropy, strong twin border mobility, and tunable magnetic and martensite transition temperatures. For the study on superparamagnetic (SPM) and paramagnetic (PM) nature changes in the alloys with respect to the σ-B curves, the curves show the deviation in between 26 and 34 °C. Since the alloy also shows a martensitic transformation temperature change in the same temperature range, this serves as a justification for the curves formed. Large changes in ΔSm and a higher RC value at x = 4 are desirable properties for applications in magnetic refrigeration. It is observed that the Cp is used to determine S_m and T_{ad} in the alloys. The value of S_m helps in identifying the value change of the inverse MCE effect in the alloy, and the adiabatic temperature change along with σ helps in identifying the origin and the validity in the magnetic properties to establish the reverse magnetic characteristics. The transition temperature varies with Cp and B; when austenite's sigma value is larger than martensite's, this shift occurs. Phonon fluctuation at the transformation temperature causes the martensite-phase transition. Increasing the sigma with B favors the phase change of the cubic structure and reduces phonon instability by coupling the magnetic and vibrational degrees of freedom. With the increase in the value of B, the transition temperature drop is seen.

In isothermal magnetization curves, the presence of a rather substantial (MR)/B value at both low and high magnetic fields and temperatures near to the TA point indicates that the current Heusler alloys composed of tiny crystallites have considerable promise for both low and high magnetic field MR applications. The inverse magnetocaloric curves also establish that the alloy shows desirable results around the transformation temperature and thus these alloys, if extrapolated on a larger scale, can be an ideal replacement for refrigeration applications.

Author Contributions: Conceptualization, S.N.S. and A.A.P.; methodology, S.N.S.; software, S.N.S.; validation, A.A.P., S.S. and M.B.R.N.; formal analysis, S.N.S.; investigation, S.N.S.; resources, S.N.S.; data curation, S.N.S.; writing—original draft preparation, S.N.S.; writing—review and editing, S.N.S. and K.B.M.; visualization, S.N.S.; supervision, M.B.R.N. and S.S.; project administration, M.B.R.N. All authors have read and agreed to the published version of the manuscript.

Funding: This research received no external funding.

Acknowledgments: INUP: Centre for Nano Science and Engineering (CeNSE), Indian Institute of Science, Bangalore, Karnataka, India.

Conflicts of Interest: The authors declare no conflict of interest.

References

1. Everhart, W.; Newkirk, J. Mechanical properties of Heusler alloys. *Heliyon* **2019**, *5*, e01578. [CrossRef] [PubMed]
2. Heusler, F. *Über Manganbronze und über die Synthese Magnetisierbarer Legierungen aus Unmagnetischen Metallen*; Angewandte Chemie: Berlin, Germany, 1904; pp. 260–264.
3. Kirat, G.; Kizilaslan, O.; Aksan, M.A. Magnetoresistance properties of magnetic Ni-Mn-Sn-B shape memory ribbons and magnetic field sensor aspects operating at room temperature. *JMMM* **2019**, *477*, 366–371. [CrossRef]
4. Graf, T.; Felser, C.; Parkin, S.S.P. Progress in Solid state chemistry simple rules for the understanding of Heusler compounds. *Prog. Solid State Chem.* **2011**, *39*, 1–50. [CrossRef]
5. Notonegoro, H.A.; Ferdian, D.; Prasetyo, Y.; Manaf, A. Microstructure analysis of synthesized iron substituted $Ni_{44}Fe_6Mn_{32}Al_{18}$ Heusler alloy. *AIP Conf. Proc.* **2016**, *1729*, 020036. [CrossRef]
6. Yu, B.; Liu, M.; Egolf, P.W.; Kitanovski, A. A review of magnetic refrigerator and heat pump prototypes built before the year. *Int. J. Ref.* **2010**, *33*, 1029–1060. [CrossRef]
7. Ghosh, A.; Mandal, K. Effect of structural disorder on the magnetocaloric properties of Ni-Mn-Sn alloy. *App. Phy. Lett.* **2014**, *104*, 031905. [CrossRef]
8. Xuan, H.C.; Xie, K.X.; Wang, D.H.; Han, Z.D.; Zhang, C.L.; Gu, B.X.; Du, Y.W. Effect of annealing on the martensitic transformation and magnetocaloric effect in $Ni_{44.1}Mn_{44.2}Sn_{11.7}$ ribbons. *App. Phy. Lett.* **2008**, *92*, 242506. [CrossRef]
9. Kumar, S.; Vinodh, R.K.; Singh, M.; Manivel Raja, A.; Bysakh, S.K.; Mahendran, M. Microstructure and nanomechanical properties of Mn-rich Ni–Mn–Ga thin films. *Intermetallics* **2016**, *71*, 57–64. [CrossRef]
10. Peruman, K.V.; Chokkalingam, R.; Mahendran, M. Annealing effect on phase transformation in nano structured Ni–Mn–Ga ferromagnetic shape memory alloy. *Phase. Transit.* **2010**, *83*, 509–517. [CrossRef]
11. Taubel, A.; Gottschall, T.; Fries, M.; Riegg, S.; Soon, C.; Skokov, K.P.; Gutfleisch, O. A comparative study on the magnetocaloric properties of Ni-Mn-X (-Co) Heusler Alloys. *Phys. Status Solidi* **2018**, *255*, 1700331. [CrossRef]
12. Titov, I.; Acet, M.; Farle, M.; González-Alonso, D.; Mañosa, L.; Planes, A.; Krenke, T. Hysteresis effects in the inverse magnetocaloric effect in martensitic Ni-Mn-In and Ni-Mn-Sn. *J. App. Phy.* **2012**, *112*, 073914. [CrossRef]
13. Li, Z.; Jing, C.; Chen, J.; Yuan, S.; Cao, S.; Zhang, J. Observation of exchange bias in the martensitic state of Ni 50 Mn 36 Sn 14 Heusler alloy. *App. Phy. Lett.* **2007**, *91*, 112505. [CrossRef]
14. Czaja, P.; Chulist, R.; Szczerba, M.J.; Przewoźnik, J.; Olejnik, E.; Chrobak, A.; Maziarz, W.; Cesari, E. Magnetostructural transition and magnetocaloric effect in highly textured Ni-Mn-Sn alloy. *J. App. Phy.* **2016**, *119*, 165102. [CrossRef]
15. Long, Y.; Zhang, Z.Y.; Wen, D. Phase transition processes and magnetocaloric effects in the Heusler alloys NiMnGa with concurrence of magnetic and structural phase transition. *J. App. Phy.* **2012**, *98*, 046102. [CrossRef]
16. Basso, V.; Sasso, C.P.; Skokov, K.P.; Gutfleisch, O.; Khovaylo, V.V. Hysteresis and magnetocaloric effect at the magnetostructural phase transition of Ni-Mn-Ga and Ni-Mn-Co-Sn Heusler alloys. *Phys. Rev.* **2012**, *85*, 014430. [CrossRef]
17. Yüzüak, E. The magnetothermal characterization of Ni-Cu-Mn-Sn alloy. *Mater. Res. Bull.* **2021**, *142*, 111398. [CrossRef]
18. Guo, J.; Zhong, M.; Zhou, W.; Zhang, Y.; Wu, Z.; Li, Y.; Zhang, J.; Liu, Y.; Yang, H. Grain size effect of the γ phase precipitation on martensitic transformation and mechanical properties of Ni–Mn–Sn–Fe Heusler alloys. *Materials* **2021**, *14*, 2339. [CrossRef]
19. Zhao, X.G.; Tong, M.; Shih, C.W.; Li, B.; Chang, W.C.; Liu, W.; Zhang, Z.D. Microstructure, martensitic transitions, magnetocaloric, and exchange bias properties in Fe-doped Ni-Mn-Sn melt-spun ribbons. *J. App. Phy.* **2013**, *13*, 913. [CrossRef]
20. Stevens, E.; Toman, J.; Kimes, K.; Chernenko, V.; Wojcik, A.; Maziarz, W.; Chmielus, M. Microstructural evaluation of magnetocaloric Ni-Co-Mn-Sn produced by directed energy deposition. *Microsc. Microanal.* **2016**, *3*, 1774–1775. [CrossRef]
21. Deltell, A.; Escoda, L.; Saurina, J.; Suñol, J.J. Martensitic Transformation in Ni-Mn-Sn-Co Heusler Alloys. *Metals* **2015**, *2*, 695–705. [CrossRef]
22. Moya, X.; Mañosa, L.; Planes, A.; Krenke, T.; Duman, E.Y.Ü.P.; Acet, M.; Wassermann, E.F. Calorimetric study of the inverse magnetocaloric effect in ferromagnetic Ni–Mn–Sn. *J. Mag. Mag. Mater.* **2007**, *316*, 572–574. [CrossRef]
23. Kamantsev, A.P.; Koledov, V.V.; Mashirov, A.V.; Dilmieva, E.T.; Shavrov, V.G.; Cwik, J.; Los, A.S.; Nizhankovskii, V.I.; Rogacki, K.; Tereshina, I.S.; et al. Magnetocaloric and thermomagnetic properties of $Ni_{2.\,18}Mn_{0.\,82}Ga$ Heusler alloy in high magnetic fields up to 140 kOe. *J. App. Phy.* **2015**, *117*, 163903. [CrossRef]
24. Fukushima, K.; Sano, K.; Kanomata, T.; Nishihara, H.; Furutani, Y.; Shishido, T.; Ito, W.; Umetsu, R.Y.; Kainuma, R.; Oikawa, K. Phase diagram of Fe-substituted Ni–Mn–Sn shape memory alloys. *Scr. Mater.* **2009**, *61*, 813–816. [CrossRef]
25. Wang, R.L.; Yan, J.B.; Xu, L.S.; Marchenkov, V.V.; Chen, S.S.; Tang, S.L.; Yang, C.P. Effect of Al doping on the martensitic transition and magnetic entropy change in Ni–Mn–Sn alloys. *Solid State Commun.* **2011**, *151*, 1196–1199. [CrossRef]
26. Gonzalez-Legarreta, L.; Sánchez, T.; Rosa, W.D.O.D.; García, J.; Serantes, D.; Caballero-Flores, R.; Hernando, B. Annealing influence on the microstructure and magnetic properties of Ni-Mn-In Alloys ribbons. *JSNM* **2012**, *25*, 2431–2436. [CrossRef]
27. Sepehri-Amin, H.; Taubel, A.; Ohkubo, T.; Skokov, K.P.; Gutfleisch, O.; Hono, K. Microstructural origin of hysteresis in Ni-Mn-In based magnetocaloric compounds. *Acta Mater.* **2018**, *147*, 342–349. [CrossRef]
28. Dubenko, I.; Ali, N.; Stadler, S.; Zhukov, A.; Zhukova, V.; Hernando, B.; Granovsky, A. Magnetic, magnetocaloric, magnetotransport, and magneto-optical properties of Ni–Mn–In-based Heusler alloys: Bulk, ribbons, and microwires. *Nov. Funct. Magn. Mater.* **2016**, *231*, 41–82.
29. Nambiar, S.S.; Murthy, B.R.N.; Sharma, S.; Prasanna, A.A.; Chelvane, A.J. Microstructure and mechanical properties of annealed quinary Ni-Mn-Sn-Fe-In Heusler alloy. *Eng. Sci.* **2022**, *17*, 303–308.

30. Nambiar, S.; Murthy, B.R.N.; Sathyashankara, S.; Prasanna, A.A. Vickers micro-hardness variation during change in concentration of constituent elements in $Ni_{50-x}Fe_xMn_{30}Sn_{20-y}In_y$, Heusler alloys. *Mfg. Rev.* **2022**, *9*, 4.
31. Nambiar, S.S.; Murthy, B.R.N.; Sharma, S.; Prasanna, A.A. Analysis on magnetocaloric and structural properties of heusler alloys used in magnetic refrigeration. *IJMPRED* **2020**, *10*, 29–46.
32. Sandeep, S.N.; Murthy, B.R.N.; Sathyashankara, S.; Prasanna, A.A. Martensitic transformation behavior and structural characteristics of annealed Ni-Mn-Sn-Fe-In Heusler alloy. *J. Phys. Conf. Ser.* **2021**, *2070*, 012231. [CrossRef]
33. Prasanna, A.A.; Ram, S.; Fecht, H.J. Consecutive magnetic and magnetocaloric transitions in herringbone nanostructured heusler $Mn_{50}Ni_{41}Sn_9$ alloy. *JNN* **2012**, *13*, 5351–5359. [CrossRef] [PubMed]
34. Prasanna, A.A.; Ram, S.; Ganesan, V.; Shanmukharao Samantham, S. Attenuating large magneto-entropy, heat-capacity and adiabatic temperature change in Heusler $Ni_{41-X}Mn_{50}Sn_{9+X}$ ($X \leq 1.5$) alloys. *J. Emerg. Trends Eng. Appl. Sci.* **2012**, *3*, 601–607.